SANDIA REPORT
SAND2011-5892
Unlimited Release
Printed August 2011

Eddy Sensors for Small Diameter Stainless Steel Tubes

Alfredo M. Morales, J. Brian Grant, Jack L. Skinner, Lisa E. Andersen, Benjamin Van Blarigan, Marianne E. LaFord, Henry J. Korellis

Sandia National Laboratories, Livermore, California.

Prepared by
Sandia National Laboratories
Albuquerque, New Mexico 87185 and Livermore, California 94550

Sandia is a multiprogram laboratory operated by Sandia Corporation,
a Lockheed Martin Company, for the United States Department of Energy's
National Nuclear Security Administration under Contract DE-AC04-94AL85000.

Issued by Sandia National Laboratories, operated for the United States Department of Energy by Sandia Corporation.

Available to DOE and DOE contractors from
U.S. Department of Energy
Office of Scientific and Technical Information
P.O. Box 62
Oak Ridge, TN 37831

Telephone: (865) 576-8401
Facsimile: (865) 576-5728
E-Mail: reports@adonis.osti.gov
Online ordering: http://www.osti.gov/bridge

Available to the public from
U.S. Department of Commerce
National Technical Information Service
5285 Port Royal Rd.
Springfield, VA 22161

Telephone: (800) 553-6847
Facsimile: (703) 605-6900
E-Mail: orders@ntis.fedworld.gov
Online order: http://www.ntis.gov/help/ordermethods.asp?loc=7-4-0#online

SAND2011-5892
Unlimited Release
Printed August 2011

Eddy Sensors for Small Diameter Stainless Steel Tubes

Alfredo M. Morales
Materials Chemistry
J. Brian Grant
Reliability and Electrical Systems
Jack L. Skinner, Lisa E. Andersen, Henry J. Korellis
Surety Design Engineering
Benjamin Van Blarigan, Marianne E. LaFord
Materials Chemistry

Sandia National Laboratories
P.O. Box 969
Livermore, California 94551-0969

Abstract

The goal of this project was to develop non-destructive, minimally disruptive eddy sensors to inspect small diameter stainless steel metal tubes. Modifications to Sandia's Emphasis/EIGER code allowed for the modeling of eddy current bobbin sensors near or around 1/8" outer diameter stainless steel tubing. Modeling results indicated that an eddy sensor based on a single axial coil could effectively detect changes in the inner diameter of a stainless steel tubing. Based on the modeling results, sensor coils capable of detecting small changes in the inner diameter of a stainless steel tube were designed, built and tested. The observed sensor response agreed with the results of the modeling and with eddy sensor theory. A separate limited distribution SAND report is being issued demonstrating the application of this sensor.

Acknowldegements

We would like to thank Jerry Fordham and Brian Holliday in the Machine Shop at Sandia CA for machining test samples. Peter Sharma and Jon Zimmerman helped review the manuscript.

Table of Contents

Background

Introduction

The goal of this project was to develop non-destructive, minimally disruptive techniques to inspect metal tubes. We would like to develop a stationary sensor capable of detecting changes in the wall thickness of 1/8" outer diameter (OD) 316 SS metal tubes. After some scoping work investigating capacitive inspection methods, eddy current (inductive) methods were downselected as the most promising approach for this application.

Eddy current methods are currently used in a variety of industries to non-destructively inspect metal components such as boiler tubes, aircraft aluminum skin, and a variety of conducting parts [Blitz 1997, Shull 2002]. The technique can inspect components from the inside out and from the outside in. However, current commercial eddy current sensors are designed for use on components considerably larger than our test samples and are operated while in relative motion to the test piece.

The main activities in this project were:

- Modeling of possible eddy current sensors.
- Fabrication of the most promising sensor design.
- Characterization of 1/8" OD 316 SS metal tubes of varying inner diameters (ID) using eddy current sensor.
- Comparison of the sensor data to model prediction.

The report is divided into four main sections covering background information, modeling work, experimental work, and conclusions.

Eddy Current Fundamentals

Eddy current methods are based on two fundamental electromagnetic (EM) concepts [Shull 2002]:

1. An alternating current flowing in a wire generates an alternating magnetic field that encircles the wire and points tangentially to the circles.
2. An alternating magnetic field inside a conductor produces an alternating voltage or electromotive force (EMF) in the conductor.

The Biot-Savart law describes mathematically the relationship stated in (1) above [Fleisch 2009, Shull 2002],

$$\vec{B} = \frac{\mu I}{4\pi}\int \frac{d\vec{l} \times \vec{a}_r}{r^2} \qquad \text{eqn 1}$$

where $\vec{B}$ is the magnetic field, r is the distance perpendicular from the wire to the point in space where $\vec{B}$ is to be calculated, and $\vec{a}_r$ is a unit direction vector pointing from a point on the current-carrying wire (source point) to the point in space where $\vec{B}$ is to be calculated. μ is the relative magnetic permeability and I is the current flowing through the wire. The integral is evaluated over the length l of the wire. The cross product states that $\vec{B}$ will be in a direction perpendicular to both the current along the wire and the direction vector $\vec{a}_r$. In other words, $\vec{B}$ will be circumferential to the wire.

Faraday's law of electromagnetic induction mathematically describes (2),

$$\vec{\nabla} \times \vec{E} = -\frac{\partial \vec{B}}{\partial t} \qquad \text{eqn 2}$$

where $\vec{\nabla} \times \vec{E}$ known as "the curl of the electric field $\vec{E}$" indicates that a circulating electric field is produced by a magnetic flux that changes with time. If the circulating electric field is inside a conductor with free electrical charge carriers (in the case of most metals the electrical charge carriers are electrons), a circulating current or "eddy current" results. The minus sign on the right hand side is due to Lenz's law which states that currents induced by changing magnetic flux always flow in a direction as to oppose the change in flux. As $\vec{B}$ reverses direction, the eddy currents also reverse direction.

These two concepts and equations enable us to put together and model an "eddy sensor" to examine conducting components [Shull 2002]. The operation of such sensor is illustrated qualitatively in Figure 1. We start with an eddy current probe that is basically a coil that carries an alternating electrical current (Figure 1a). This coil generates an alternating magnetic field and this magnetic field causes the coil to display a characteristic inductance L_0 which together with the characteristic resistance R_0 of the coil determine the characteristic impedance Z_0 (in units of ohms) according to

$$Z_0 = R_0 + i2\pi f L_0 + \frac{1}{i2\pi f C_o} \qquad \text{eqn 3}$$

where f is the alternating current frequency (in Hertz) and C_0 is the capacitance of the probe.

Now let's place a non-magnetic conductor, say a metal test part, in proximity to the coil (Figure 1b). Some of the alternating magnetic field penetrates the conductor and eddy current loops are induced perpendicular to the field lines (Figure 1c). These eddy currents generate their own magnetic field and according to Lenz's law this new magnetic field opposes the magnetic field from the coil.

Because of the eddy current generated magnetic fields that oppose the magnetic field initially generated by the coil, the inductance of the coil decreases and it is now denoted as L. The eddy currents dissipate heat and thus the resistance of the coil increases and it is now denoted by R. The new impedance is now given by

$$Z = R + i2\pi fL + \frac{1}{i2\pi fC_0} \qquad \text{eqn 4}$$

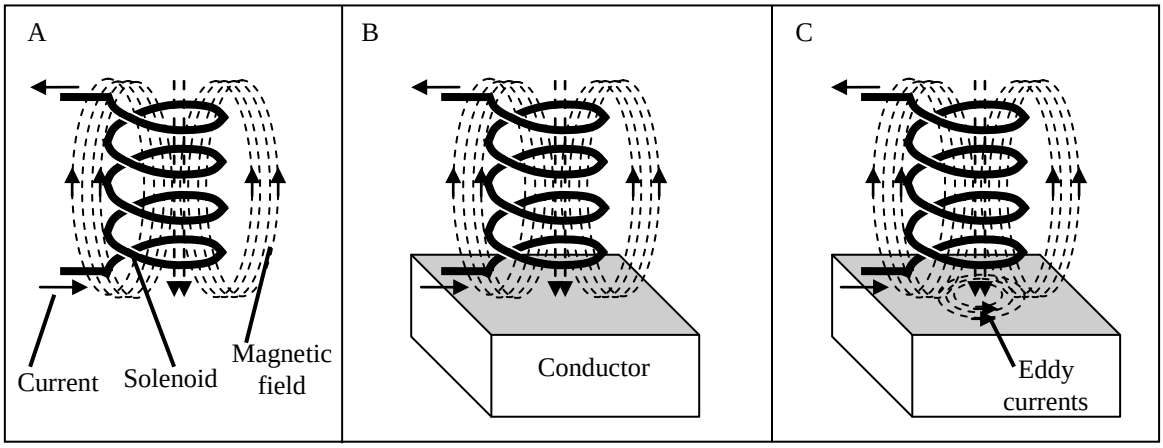

Figure 1: Qualitative operation of an eddy current sensor. (a) A first coil carries an alternating electrical current and thus an alternating magnetic field is created around the coil. (b) The coil is then placed in proximity to a non-magnetic conductor. Some of the magnetic field around the coil penetrates into the conductor. (c) Eddy currents are generated inside the conductor and generate their own magnetic field that opposes the field generated by the coil.

where we assume that the capacitance C_0 has not changed.

It is useful to consider the behavior of the eddy sensor using an impedance plane diagram (capacitance will now be ignored) [Shull 2002]. Figure 2a shows a non-normalized impedance plane for a non-magnetic solid rod with an encircling eddy sensor [Shull 2002]. The plot shows the value of ωL versus R as the conductivity of the solid rod increases ($\omega = 2\pi f$). In this plot, Z is given by the length of the vector that starts at the origin and ends on the curve. The free space inductance and resistance intrinsic to the coil are given by L_0 and R_0 respectively. As the conductivity of the rod increases, the magnitude of the secondary field created by the eddy currents increase and since the secondary field opposes the original field at the coil, the inductance of the coil decreases. Initially, more resistance is added to the coil as the eddy currents in the rod dissipate energy. However, at some point on the curve, the conductivity of the sample has increased enough that the added resistance starts to decrease. At the limit of infinite conductivity in the rod, there is no added resistance from the rod and the value of the coil resistance goes back to the initial free space value R_0. At that point the secondary magnetic field generated at the sample is equal in magnitude and opposite in sign to the original field at the coil and the value of the inductance goes to zero.

The plot in Figure 2a must be modified every time the coil dimensions or test frequency are changed. Thus, it is more useful to use a normalized plot that is immune to changes in the system (Figure 2b). This plot is generated by using the following transformations,

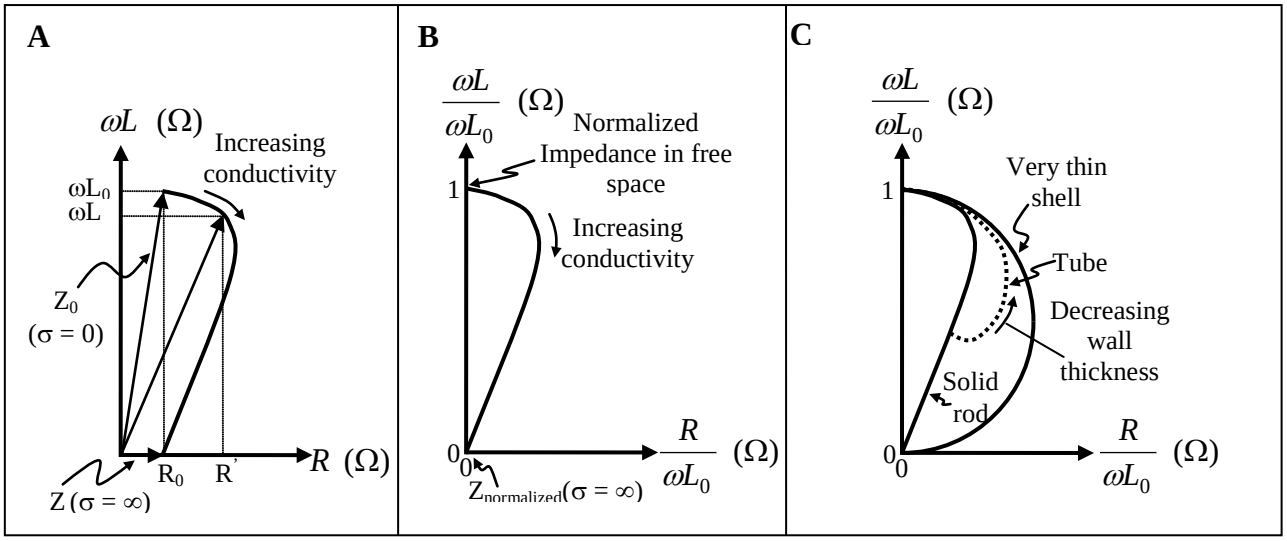

Figure 2: (a) Non-normalized impedance plane diagram for a solid rod with an encircling eddy sensor. (b) Normalized impedance plane diagram for a solid rod with an encircling eddy sensor. (c) Material thickness effect on the normalized impedance plane for a solid rod, a tube, and a very thin shell [Shull 2002].

$$R = R_{total} - R_0 \qquad \text{eqn 5}$$

$$Z_{normalized} = \frac{R}{\omega L_0} + i\frac{\omega L}{\omega L_0} \qquad \text{eqn 6}$$

where R_{total} is the total resistance and R is the additional resistance from eddy currents in the rod. The normalized plot basically shows the normalized additional resistance as the abscissa and the normalized total inductance as the ordinate.

Figure 2c shows the effect of material thickness on the normalized impedance plane for a solid rod, a tube, and a very thin shell. The normalized impedance curve for the solid rod (solid trace) was discussed above. The extreme case of a very thin shell generates an impedance curve (solid trace) that is a perfect semicircle. This shape is due to the fact that a shell thinner than the penetration depth has a more uniform response to an increase in conductivity than a rod or tube (see Shull 2002 for more information). The dashed line shows the response of a tube as the sidewall thickness decreases. When the sidewall is thick, the tube behaves as a rod. Once the sidewall becomes considerably thinner than the penetration depth at a given frequency, the dashed line coincides with the impedance trace for a thin shell. For sidewall thicknesses in between these two extremes, the inductance of the coil increases as the sidewall thickness decreases because less secondary field is produced by the decreasing eddy current. The resistance first increases from the solid rod value and it eventually approaches the resistance value of a thin shell.

The changes in inductance, resistance, and impedance of the coil can be measured using a variety of modern electronic test instruments. The coil can also be placed in series or in parallel with a capacitor and the resulting LC circuit will resonate at different frequencies and with different gains depending on the resistance and inductance of the coil in the presence of the non-magnetic conductor.

Modeling

Methods

Modeling Codes

The primary code used to calculate the response of candidate eddy current sensors by solving equations 1 through 4 above as well as all other governing EM equations is the ASC code Emphasis/EIGER. The moment method code is extremely versatile. In general, however, the moment method algorithm can lead to instabilities at low frequencies. Specifically, the summation of contributions has significant cancellation of terms at low frequencies, and, thus, round-off can lead to instabilities. To avoid this, a well known technique (Loop/Star) was implemented to construct alternative basis functions that are not susceptible to this problem. Due to the flexibility designed into EIGER, only minor modifications to the code were needed for this extension. However, a significant effort outside the scope of this project was required to create a new, auxiliary tool that converts a traditional model into a Loop/Star model.

The modeling of the small tubes and their sensors utilized this new capability. The dramatic improvement in accuracy changed the results from looking like noise to picture-perfect. Additional, minor enhancements included extensions to material definitions to allow for explicit specification of conductivity, and the specification of loads in terms of their RLC equivalents to introduce frequency dependence.

Relevance of Modeling Effort to Sensor Development

The modeling of eddy sensors applied to small diameter stainless steel tubes allows one to downselect the most sensitive coil design and sample-coil geometry and also provides a foundation for understanding the measured data. Of interest was observing total metal mass, specifically, detecting differences between samples of tubes with different wall thick-nesses or interior blockages. Both one- and two-coil configurations were modeled. The pipes used in the model utilized the materials parameters for non-magnetic 316 stainless steel.

One-Coil Configurations

The primary configuration investigated consisted of a single axially wound coil. A second configuration consisted of an identical coil, but placed transversely to the pipe. It is referred to as a pancake coil because it is laid at against the pipe. This pancake configuration is not reported under this one-coil configuration because its behavior is not suficiently different from the corresponding two-coil configuration reported later. Typical single coil configurations are shown in Figure 3.

The coils used in both the one coil and the two coil models had 8 wraps in a single layer. More wraps, or more layers, would not qualitatively change the results, though it would

introduce challenges for the simulation. The coil was modified with a fixed-value capacitor, added in series with the coil, to establish a resonant frequency.

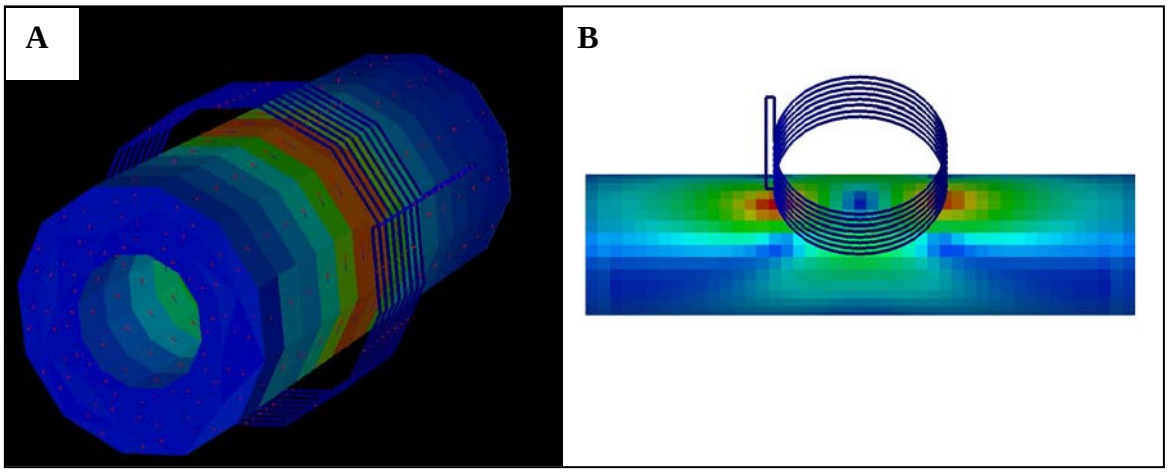

Figure 3: (a) Eddy current intensity (color) and flow (arrows) for single coil around small tube. (b) Eddy current intensity (color) for single coil pancake configuration.

Two-Coil Configurations

Two generic configurations were studied for the two coil case: an axial configuration where the coils were wrapped around the pipe, and a pancake configuration in which the coils were laid against the pipe with their axes perpendicular to the axis of the pipe. In some instances, the pipe had a solid blockage of 1/32" thick non-magnetic stainless steel, the same thickness as the pipe walls. These configurations had a primary coil driven with a constant voltage swept from 60KHz to 70KHz, and a secondary, passive coil that had a 1M Ohm load attached. All coils had radius R comparable to the experimental setup. The location of the primary coil and the separation between coils were used as parameters in the study. The former were labeled Z_{axial} or $Z_{pancake}$ depending on the generic configuration of the coil alignments and were measured from the center of the pipe's blockage to the center of the coil; the latter was labeled $Z_{secondary}$ and was measured relative to the primary coil.

Results and Discussion

Penetration Depth and Eddy Current Theory

Industry experts [at GE] indicated that 300-700 KHz would be an appropriate frequency range. However, at these small dimensions, the simulations demonstrated much better sensitivity at 30-70 KHz. At this lower frequency range the penetration depth (skin depth) given by the formula,

$$\delta = \frac{1}{\sqrt{\pi \mu \sigma f}} \qquad \text{eqn 8}$$

where δ is the skin depth, μ is the magnetic permeability of the material, σ is the electrical conductivity of the material, and f is the frequency, is roughly 2-3 times greater than the penetration depth at the higher frequency range (Figure 6).

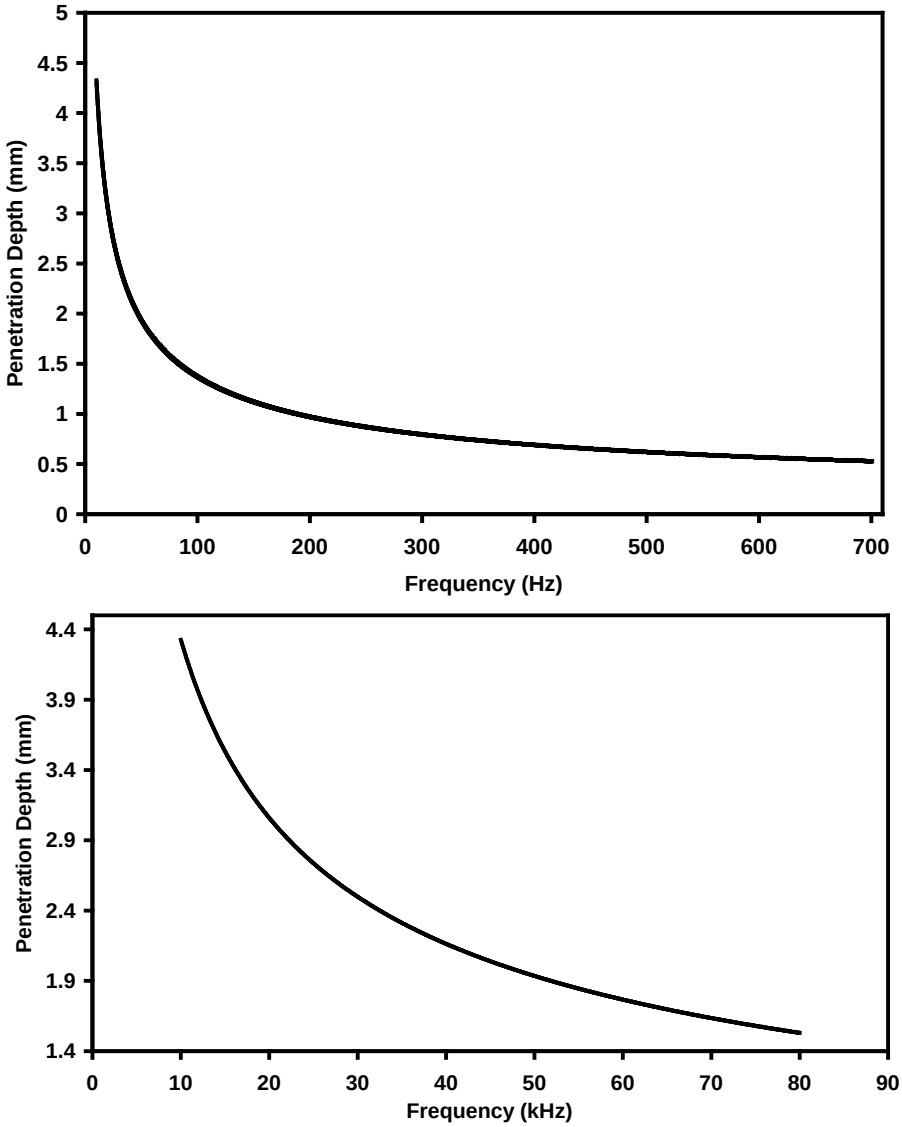

Figure 6: Skin depth for stainless steel at two different frequency ranges.

At these lower frequencies the eddy current penetration is much more uniform, as shown in Figure 3a. This is because at the resonance frequency of the model circuit (77.6 kHz) the penetration depth is 1.55 mm while at the resonance frequency of the measurement circuit (66.9 kHz) the penetration depth is 1.67 mm. The OD of the test sample is 1/8 = 0.125 inch (or 3.175 mm), and the ID ranges from 0.059 inch to 0.091 inch (or 1.50 mm to 2.31 mm). The wall thickness is then 0.43 mm to0.83 mm, smaller than the penetration depth at either frequency. This makes our samples good approximations to “thin wall tubes” and the region of the axial sensor, normalized impedance plane that applies to this type of tube is shown in Figure 7. Thus, eddy current theory predicts that as the wall

thickness of a thin wall tube decreases, there will be a small increase in the inductance of the axial sensor and a concomitant large decrease in the resistance of the sensor.

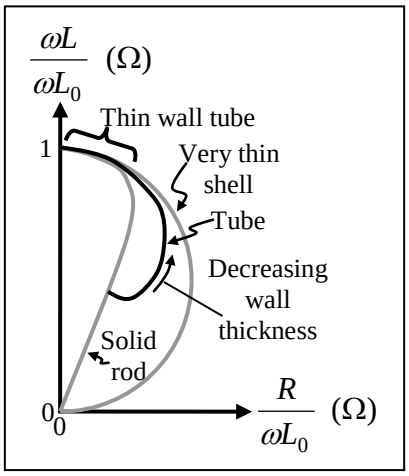

Figure 7: Normalized impedance plane for tube showing the effect of wall thickness, the impedance locus for a thin wall tube, and the bounding curves for a solid rod and for a thin shell.

One-Coil Configurations

The model shows that the eddy currents flow circumferentially and are confined primarily to the region near the coil (Figure 3a). The darkest blue indicates no current and the brightest red indicates a maximum. With respect to sensitivity, the higher frequency simulations show admittance changes of less than 1% for an increased I.D. of 20%, while the more uniform penetration of the lower frequencies produces a much larger effect on the current flowing in the coil (Figure 8).

The plot shown in Figure 8 plots admittance versus frequency for a series circuit (Figure 5a). The impedance of the series circuit is given by [Horowitz 1998],

$$Z_{series} = R + i\omega L + \frac{1}{i\omega C} \qquad \text{eqn 9}$$

and the admittance is,

$$Y_{series} = \frac{1}{Z_{series}} \qquad \text{eqn 10}$$

The magnitude of the admittance is then given by,

$$\left|Y_{series}\right| = \left|\frac{1}{Z_{series}}\right| = \frac{1}{\left|Z_{series}\right|} = \frac{1}{\sqrt{R^2 + \left(\omega L - \frac{1}{\omega C}\right)^2}} \qquad \text{eqn 11}$$

Thus, according to eqn. 11, as R decreases, the magnitude of the admittance Y_{series} will increase.

Two effects are apparent in the modeling results shown in Figure 8: the admittance increases (i.e. the amount of current flowing increases) and the frequency at which it peaks decreases as the wall thickness of the tube decreases. The increase in admittance results from changes in the ohmic losses of the eddy currents flowing through the pipe walls, where less volume of material (thinner walls) carries less current and thus produces less loss/more admittance as predicted by equation 11. The lower total loss is due to the fact that the thin wall tube has uniform current density running through its cross-section and so less cross-section means less total current. The decrease in frequency is caused by changes in the strength of the (opposing) magnetic field reflected back to the coil, which decreases as the volume of metal decreases. This causes the total inductance to slowly increase (Figure 7) which then causes the resonance frequency to decrease (Eqn. 8).

The changes in loss is more pronounced than the frequency shift. This would be even more pronounced with realistic (i.e., lossy and, therefore, lower Q) coils for which the peak location is more difficult to identify. Thus, admittance amplitude when in series or impedence amplitude when in parallel is the more useful quantity to observe in any final application.

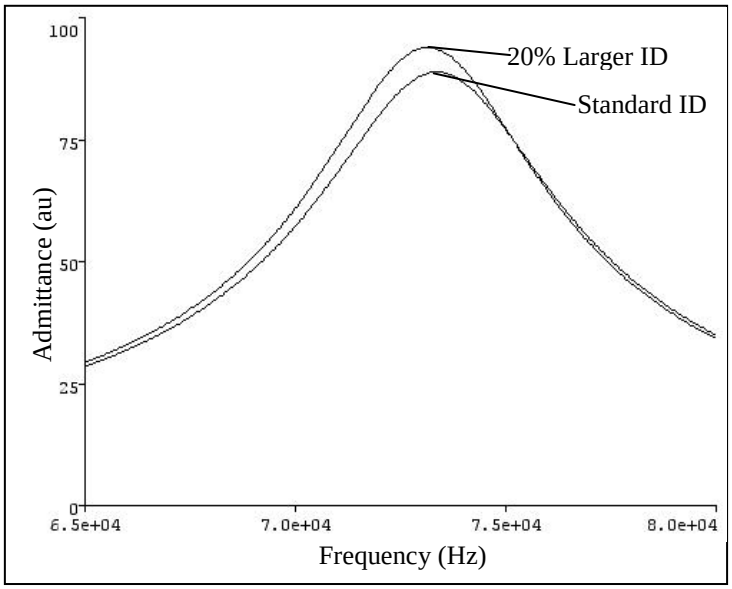

Figure 8: Simulated response for single coil around small tube with standard (0%) and 20% larger I.D.

Two-Coil Configurations

Figure 9 shows the modeling results for the 2-coil geometries when trying to sense a blockage in the pipe. The important result from this 2-coil study is that the secondary coil does not measure changes that the primary cannot; it does not contribute any information in this passive mode. While the secondary coil could be also be driven, in a common or differential mode, it is doubtful that much variation would be observed because the coils are coupling almost entirely outside the extremely small pipe. The secondary coil is not significantly altering the field penetration in the pipe as was hoped (though it does add a significant amount of inductance). This is not to say that, in a real system, it couldn't increase signal-to-noise ratios by separating driver and sensor functions. The graphs clearly show that the pancake configuration has a much higher Q. However, since the source of loss is the pipe, it indicates that the pancake configuration interacts with a much smaller volume of the pipe. Thus, as observed in the graphs, the axial configuration exhibits a much stronger sensitivity to the blockage than the pancake alignment does. The latter being almost imperceptible.

The pancake coil could be made more effective with a core of iron or other material with a high magnetic permeability. If the core touches the pipe and has a diameter equal to or smaller than the pipe it could help focus the magnetic fields into the pipe and enhance the eddy currents. Such a core is not possible in the axial configuration. However, a smaller diameter coil, which would force the magnetic fields deeper into the pipe, could be advantageous in that configuration.

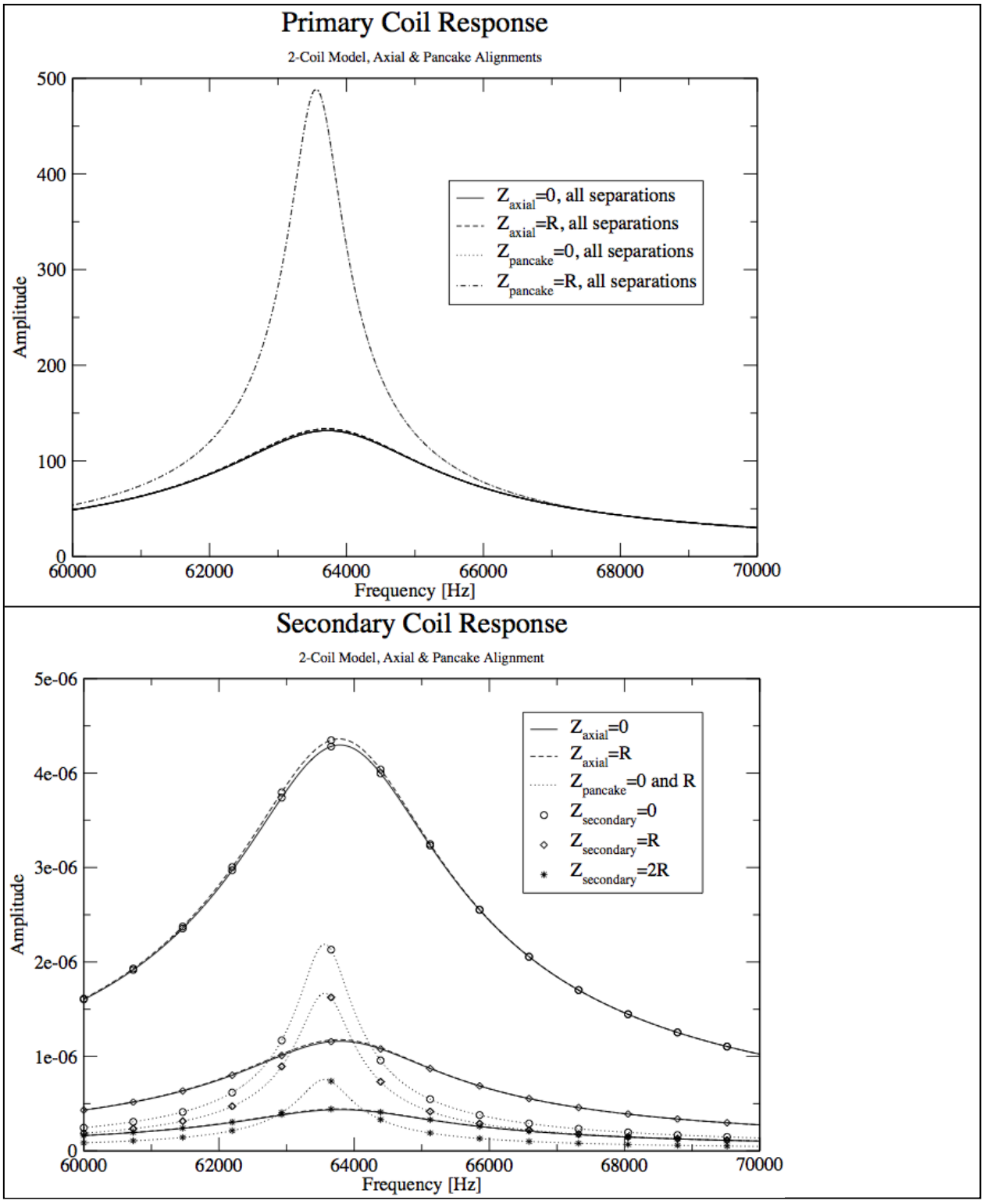

Figure 9: Two-coil responses. The locations of the primary coil were labeled Z_{axial} or $Z_{pancake}$ depending on the generic configuration of the coil alignments and were measured from the center of the pipe's blockage to the center of the coil; the separation between coils was labeled $Z_{secondary}$ and was measured relative to the primary coil.

Experiments

Methods

Sensor Fabrication

The sensors were fabricated using Delrin (Figure 4a), a machinable polyacetal, as the bobbin material and 32 gauge (0.2743 mm diameter) copper wire as the solenoid material. 200 turns of wire were wound around the bobbin using a wire winder to ensure a tight, uniform solenoid (Figs. 4b and 4c). After winding, the wire was affixed in place using a clear, five minute epoxy.

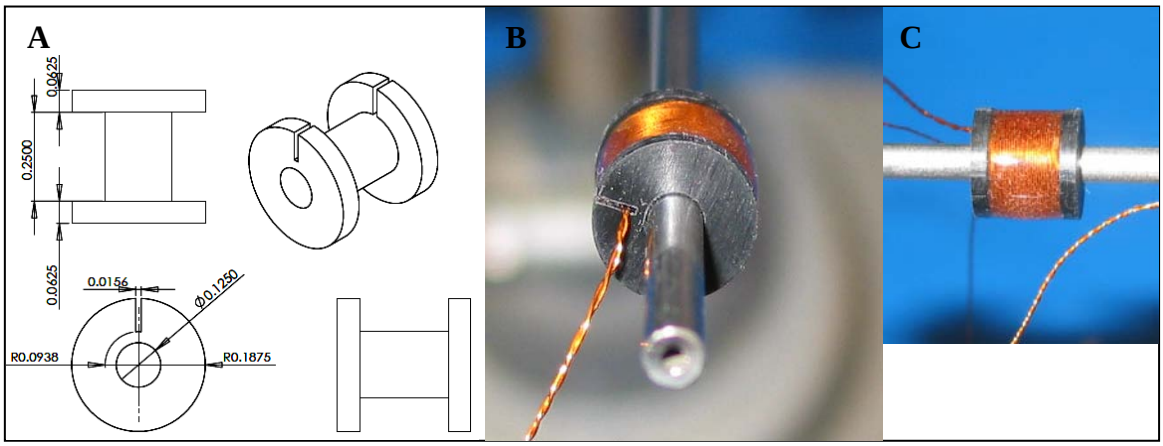

Figure 4: (a) Schematic showing dimensions of Delrin bobbin. (b) and (c) are two different views of sensor threaded through a 1/8 OD, 316 stainless steel tube.

Test Sample fabrication

The samples used to characterize the performance of the eddy current sensor were tubes machined from 316 SS rod stock. The tubes OD was 1/8 inch and the insides of the tubes were drilled using an external gun drill to ensure that the hole was straight, concentric, and accurately sized. Three tubes for each of seven different ID sizes were fabricated.

Measurement Equipment and Circuitry:

The impedance and gain of the sensors were measured using two different impedance analyzers:

HP4194A: This is an older impedance gain analyzer capable of measuring impedance and gain as a function of frequency.

Agilent 4294A: This is a more modern precision impedance analyzer also capable of measuring impedance and gain as a function of frequency.

Two simple circuits were considered for modeling and measuring the interaction of the coil sensor with the test sample, a series circuit and a parallel circuit (Figure 5). For the modeling work, the sensor coil was connected in series with a capacitor (Figure 5a) and the following initial values were used,

$$R_{0,model} = 0.001\Omega$$
$$L_{0,model} = 0.32\mu H$$
$$C_{0,model} = 15\mu F$$

The changes in the inductance and resistance of the sensor coil and the lumped circuit admittance were then calculated as the coil interacted with the stainless steel test sample. Admittance is the inverse of impedance and for a series circuit it is at a maximum at the resonance frequency (i.e. the impedance is at a minimum). The capacitance was held constant at 15μF.

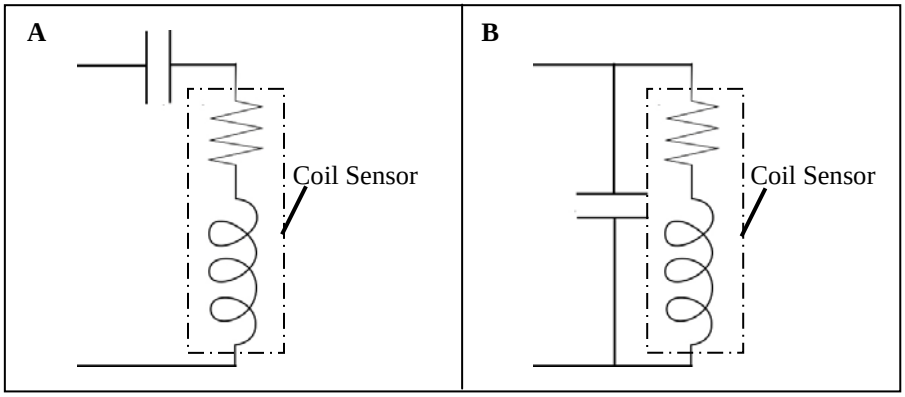

Figure 5: The eddy current coil sensor can be connected in (a) series or in (b) parallel.

The R and L at each frequency were extracted from the series model with the capacitance held constant at 15 μF and applied to a parallel circuit model (Figure 5b) and the results compared to the experimental results. The impedance is at a maximum in a parallel circuit at the resonance frequency (i.e. the admittance is at a minimum). Note that plotting admittance for a series circuit is qualitatively equivalent to plotting impedance for a parallel circuit with the same R, L, and C.

Experimental measurements were carried out using a parallel circuit configuration (Figure 5b). In a typical experiment, the impedance and gain were measured as a function of frequency for a 200 turn bobbin connected in parallel with a 39 nF capacitor. The free space capacitance of the 200 turn bobbin was measured at 145 μH. 401 measurements were taken at frequencies equally spaced from 10 kHz to 80 kHz. In each measurement run, ten measurements were taken and then averaged at each frequency. Four measurement runs were carried out and then averaged at each frequency. Thus the impedance and gain at every frequency was measured a total of 40 times to reduce noise. Virtually identical results were obtained with the HP and the Agilent instruments.

Whether a circuit is in series or in parallel, the resonance frequency when the circuit is far away from a conductor (free space state) is given by,

$$f_{res} = \frac{1}{2\pi\sqrt{LC}} \qquad \text{eqn 7}$$

and thus we expect our free space model circuit to resonate at 72.6 kHz and our free space experimental circuit to resonate at 66.9 kHz.

Results and Discussion

Sensor Characterization

The 200 turn sensor was characterized in a parallel circuit configuration (Figure 5b). The impedance of such circuit is calculated by adding the impedances of the capacitor and of the inductor legs in parallel [Horowitz 1998],

$$Z_{parallel} = \frac{1}{\frac{1}{Z_{capacitor}} + \frac{1}{Z_{inductor}}} \qquad \text{eqn 12}$$

$$Z_{parallel} = \frac{1}{iwC + \frac{1}{R + i\omega L}} = \frac{1}{iwC + \frac{R - i\omega L}{R^2 + \omega^2 L^2}}$$

$$= \frac{1}{\frac{R}{R^2 + \omega^2 L^2} + i\omega\left(C - \frac{L}{R^2 + \omega^2 L^2}\right)}$$

$$\left|Z_{parallel}\right| = \frac{1}{\sqrt{\left(\frac{R}{R^2 + \omega^2 L^2}\right)^2 + \omega^2\left(C - \frac{L}{R^2 + \omega^2 L^2}\right)^2}} \qquad \text{eqn 13}$$

Thus, according to eqn 13, as R decreases, the magnitude of the impedance $Z_{parallel}$ will increase as the circuit becomes a perfect LC resonator.

Figure 10 shows the typical response of the 200 turn sensor when connected in parallel with a 39 nF capacitor.

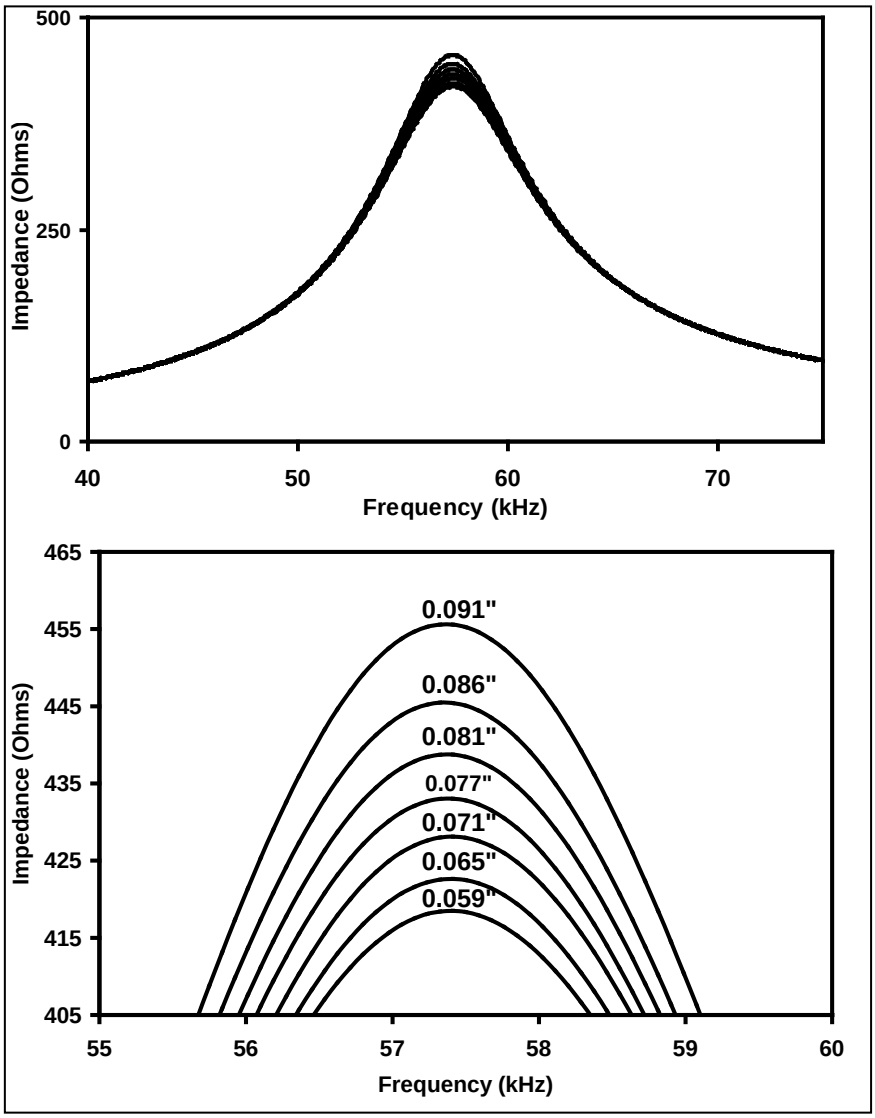

Figure 10: LC impedance as a function of frequency for the 200 turn copper bobbin connected in parallel with a 39 nF capacitor. 316 SS tubes of ID's ranging from 0.059" to 0.091" were threaded through the middle of the bobbin sensor.

The data clearly shows that the impedance systematically varies with changes in the ID of the tube. The variation in peak impedance as a function of ID is shown in Figure 11.

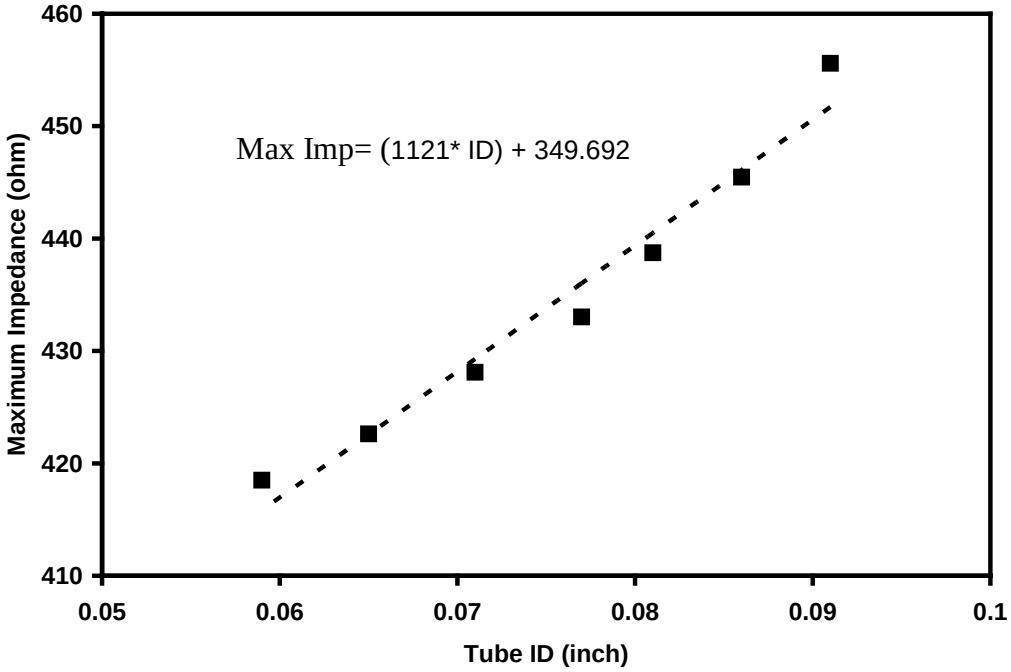

Figure 11: Maximum Impedance for data from Figure 8 as a function of tube inner diameter.

Thus the experimental data shows that as the tube ID increases (wall thickness decreases), the maximum impedance increases as shown both in the model and by normalized impedance plane theory. The linear fit through the arguably-not-quite-linear data shown in Figure 11 indicates that the maximum impedance of the current sensor geometry changes by 1 ohm for every 0.001" (25.4 micron) of change in the tube ID.

We attempted to extract the resonance frequency for each of the pipe ID's shown in Figure 10 and to generate a plot that would show a systematic increase in inductance (a decrease in resonance frequency) as the ID increased. However, as the model and eddy current theory indicated the change in inductance and in resonance frequency were too small to easily and reliably detect.

Conclusion

In this project we successfully,

- Modified Sandia's Emphasis/EIGER code to allow for the modeling of eddy current bobbin sensors near or around 1/8" OD stainless steel tubing.
- Modeled and determined that an eddy sensor based on a single axial coil could effectively detect changes in the ID of a stainless steel tubing
- Designed, built and tested a bobbin sensor that demonstrated the ability to detect small changes in the ID of a stainless steel tube.
- Compared the observed sensor response to the modeling results and to eddy sensor theory.

This project has laid the foundation to model, design, fabricate, and test minimally disruptive, static eddy current sensors that can non-destructively examine small metal components in critical Sandia applications.

A separate limited distribution SAND report is being issued demonstrating the application of this sensor.

References

Blitz 1997: Blitz, J., “Electrical and Magnetic Methods of Non-destructive Testing”, pp. 94-131, Chapman & Hall, New York, NY, 1997.

Fleisch 2009: Fleisch, D., “ A Student’s Guide to Maxwell’s Equations”, Cambridge University Press, Cambridge, UK, 2009.

Horowitz 1998: Horowitz, P., Hill, W., “The Art of Electronics”, Cambridge University Press, Cambridge, UK, 1998.

Shull 2002: Shull, P.J., “Theory, Techniques, and Applications”, pp. 261-368, Marcel Dekker, Inc., New York, NY, 2002.